Applications of Computational Fluid Dynamics in Cardiovascular Disease

Gianluca Rigatelli[1,*], Marco Zuin[2], Sarthak Agarwal[3], Vivian Nguyen[4], Cardy Nguyen[5], Sanyaa Agarwal[6], and Thach Nguyen[7,8]

[1]*Cardiovascular Diagnosis and Endoluminal Interventions Unit, Rovigo General Hospital, Rovigo, Italy*
[2]*Section of Internal and Cardiopulmonary Medicine, University of Ferrara, Ferrara, Italy*
[3]*The University of Chicago, Pritzker School of Medicine, Chicago IL, USA*
[4]*University of Texas, Southwestern Medical School, Dallas, TX, USA*
[5]*University of California, at Berkeley, CA, USA*
[6]*Chesterton HS, Chesterton IN, USA*
[7]*Cardiovascular Research Department, Methodist Hospital, Merrillville IN, USA*
[8]*Tan Tao University, School of Medicine, Long An, Vietnam*

*Corresponding author: Gianluca Rigatelli, MD, Ph.D., EBIR
Cardiovascular Diagnosis and Endoluminal Interventions Unit, Rovigo General Hospital, Rovigo, Italy
Email: jackyheart@libero.it

Article history: Manuscript received July 02, 2022; revised manuscript received September 18, 2022; accepted September 13, 2022.

ABSTRACT Computational fluid dynamics (CFD), alone or coupled with the most advanced imaging tools, allows for the assessment of blood flow patterns in cardiovascular disease to both understand their pathophysiology and anticipate the results of their surgical or interventional repair. CFD is a mathematical technique that characterizes fluid flow using the laws of physics. Through the utilization of specific software and numerical procedures based on virtual simulation and/or patient data from computed tomography, resonance imaging, and 3D/4D ultrasound, models of circulation for most CHDs can be reconstructed. CFD can provide insight into the pathophysiology of coronary artery anomalies, interatrial shunts, coarctation of the aorta and bicuspid aortic valve, tetralogy of Fallot and univentricular heart, valvular heart disease, and aortic disease. In some cases, CFD may be able to simulate different types of surgical or interventional repairs, allowing for the tailoring of treatment accordingly.

KEYWORDS Cardiovascular disease; Computer simulations; Computational fluid dynamics; Pathophysiology; Therapy

INTRODUCTION

Computational fluid dynamics (CFD) is a well-established technique used in many fields of engineering design and analysis. [1]. Notably, bioengineers have adopted CFD for studying complex physiological flows [2]. There is an increasing interest in applying these methods to cardiovascular medicine, and CFD-based techniques are increasingly used to build computer representations of the cardiovascular system in both healthy and pathological conditions [3]. The aim of the present review is to outline the findings of CFD in the study of cardiovascular pathophysiology, as well as CFD's applications in endovascular and surgical repair planning.

COMPUTATIONAL FLUID DYNAMICS
Definition

CFD is a technique that uses computer simulations to analyze systems involving fluid flow, heat transfer, and associated phenomena (e.g., chemical reactions) [4]. CFD is suitable for a wide range of industrial and non-industrial applications, including aircraft and automotive aerodynamics, ship hydrodynamics, turbomachinery, meteorology, and biomedical engineering, among others [5]. In cardiovascular hemodynamics, CFD is usually utilized to analyze blood flow patterns within the heart and vessels by considering physical laws governing fluids. Biological effects, such as auto-regulation, healing, and growth, are seldom modeled. Specifically, the governing equations of fluid motion are the continuity equation (eq. (1)), which is derived from mass conservation, and the Navier-Stokes equations (eq. (2)), which are derived from momentum conservation, and which can be expressed in the case of an incompressible and Newtonian fluid as follows:

$$\nabla . v = 0 \qquad (1)$$

$$\rho \left[\frac{\partial v}{\partial t} + v \cdot \nabla v \right] = -\nabla p + \mu \nabla^2 v + \rho g \qquad (2)$$

where ∇ is the nabla operator, v the velocity vector, ρ is the blood density, t is the time, p is the pressure, and g is the gravity. These non-linear, partial differential equations cannot be solved analytically in the case of complex three-dimensional geometries. Thus, numerical techniques, usually based on the finite volume or finite element method, are adopted to solve the discretized form of the equations within CFD software packages [5]. First, by means of the meshing process, the fluid domain (i.e., continuum of interest) is subdivided into smaller, non-overlapping sub-domains called elements. Secondly, the governing equations are integrated over all the elements of the domain and then converted into a system of non-linear algebraic equations. Lastly, the resulting set of algebraic equations (often in the order of millions of equations) is solved iteratively using computer workstations or high-performance computing clusters. Nowadays, advancements in parallel computer processing have allowed for solutions to the governing equations of fluid motion to be calculated under non-steady conditions in complex anatomies within a reasonable computational timeframe. Typically, resolving a time-accurate expression can require one or more days of computations, considering a fluid domain discretized into one million elements (or more) and multiple cardiac cycles, which are each subdivided into hundreds of time steps [3].

CFD analysis: workflow

The main steps of a patient-specific CFD analysis are summarized in Figure 1. First, the three-dimensional geometrical model of the vascular region of interest is reconstructed from non-invasive or invasive images. Specifically, vessels and cardiac chambers are virtually reconstructed based on the measurements of vessel diameters and lengths obtained by quantitative coronary angiography, computed tomography, MRI analyses, or by processing intravascular images (i.e., intravascular ultrasound or optical coherence tomography) [6], [7]. Manual or semi-automatic segmentation algorithms, which are included in commercially available software, are used to identify the region of interest. As a result of the segmentation process, a preliminary, triangulated mesh surface representing the vessel or cardiac chamber wall is obtained. The model is subsequently optimized by applying refinement processes such as triangle reduction and smoothing operations [5]. Secondly, the obtained geometrical model is discretized (meshing process) [5]. Typically, the computational grid is characterized by tetrahedral (or hexahedral) elements within the fluid domain and a prism layer close to the wall, which is introduced to better capture the high-velocity gradients at this location. Thirdly, the set-up of the CFD simulation is defined. In particular, the physical model (e.g., unsteady flow with or without the inclusion of a turbulent model), blood properties (i.e., blood density and viscosity), initial conditions, boundary conditions, and solver settings are set. Delimiting the initial and boundary conditions, which are prescribed values of the calculated quantities (i.e., velocity and pressure) at certain times and locations, is mandatory for the resolution of the govern-
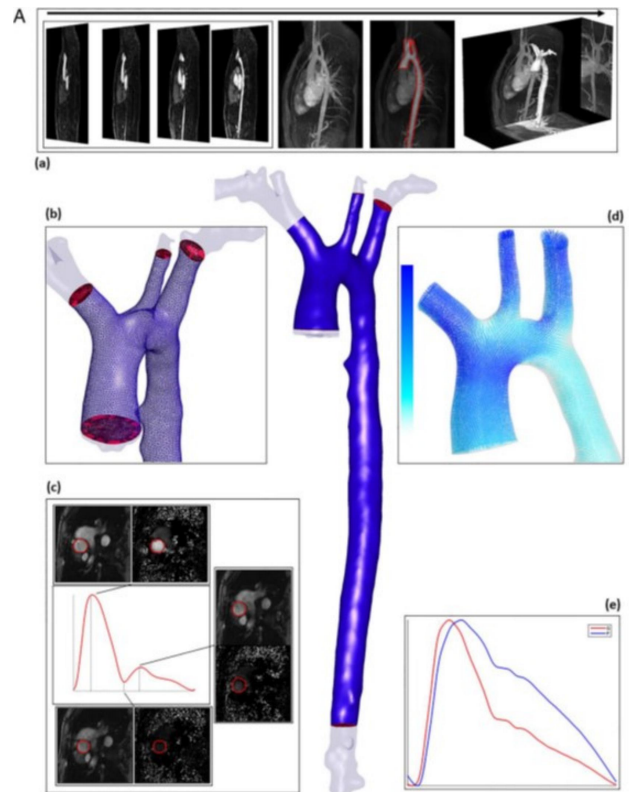

FIGURE 1. Examples of aortic (A) and coronary (B) in silico computational fluid dynamics (CFD) workflows. (A) The aorta is identified via thoracic MRI (a), segmented, and reconstructed (central image). A volumetric mesh is fabricated to fit the patient-specific geometry, shown in detail in panel (b). Accurate flow measurements are extracted from phase-contrast MRI data to inform the boundary conditions applied for CFD simulation, such as the inlet (c). The results are post-processed, and details of the flow field are shown in panel (d). 0D models are coupled at the outlets, so physiologically feasible flow-pressure relationships are computed at the outlets (e). These can be validated against other measurements, which in a preclinical scenario may be invasive. (B) (and accompanying online video) A coronary angiogram (a) is segmented (b) and reconstructed into a 3D in silico model. A surface and volumetric are fabricated to fit the patient-specific geometry (c). Physiological parameters such as pressure and flow are used to inform the boundary conditions applied for CFD simulation (d). The results (here pressure and flow) are post-processed, and useful physiological data are extracted (e). Modified from Morris PD et al. [3].

ing equations. These conditions can be derived from imaging data or experimental measurements, such as MRI data, Doppler ultrasound, catheter-based pressure, and velocity measurements, or transesophageal echocardiography. Fourth, the CFD simulation is run on a computer workstation or high-performance computing cluster by taking advantage of their parallel computing features. Lastly, once the solution of the CFD analysis is obtained, the results are post-processed in order to extract the hemodynamic quantities of interest, which are detailed in the following sub-section.

CFD analysis: quantities of interest

The main flow phenomena that can be characterized by CFD by corresponding hemodynamic quantities of interest are reported in Table 1. The hemodynamic quantities derived from both pressure and velocity fields are analyzed. The

TABLE 1. Examples of flow phenomena that can be characterized by CFD.

Parameters
Local pressures and flows
Flow distributions
Flow energy loss
Abnormal flow patterns
Re-circulating flows, stagnation flow
Wall shear stress and normal stress
Oscillatory shear index
Impact on cardiac function and vessel wall compliance
Shear stress gradient

pressure in the vessels and chambers is expressed in pascal (Pa), as per the International System of Units. The vorticity magnitude (expressed in 1/s) is defined as the magnitude of the vorticity vector; the vorticity vector expresses the rotation of a fluid element as it moves through the domain, and it may be representative of pathological conditions when substantially removed from baseline [8]. The wall shear stress (WSS) (expressed in Pa) is defined as the frictional force of flowing blood along the wall surface per unit area. WSS values deviating from baseline are indexes of abnormalities leading to thrombus formation, abnormal vessel modeling, and remodeling, and arterial damage [9]. Another important quantity to be evaluated is the power (energy per unit time, measured in watts) dissipated when the blood flows through arteries. Minimizing this loss of energy when designing or re-routing blood in surgical connections is desirable, and such an index thus may be used to predict the successful streamlining of blood flow.

CFD APPLICATIONS FOR CONGENITAL HEART DISEASE

CFD is currently applied to a variety of CHDs in order to both pathophysiology evaluation and surgical or interventional procedures planning.

Embryonic heart development

Hemodynamic processes begin shaping the growth of the developing heart from the early embryonic stages. Blood circulation starts with the beating primitive tubular heart (around the beginning of the fourth gestational week in human development) [10]. From this time on, the dynamics of blood flow determine many aspects of cardiovascular development. For instance, the formation of vessels and capillaries, and even the differences between arterial and venous phenotypes, are determined by blood flow characteristics [6]. In the heart, the relationships between blood flow and cardiac tissues also determine how the heart continues to develop [11], [12]. Understanding blood flow mechanics ultimately helps researchers to identify the causes of congenital heart malformations. Detailed CFD models of both the developing vasculature and the heart, together with experimental data on adaptations to blood flow, are starting to elucidate important aspects of the complex mechanisms by which blood flow dynamics regulate cardiovascular growth and development.

In this respect, WSS plays an important role in cardiovascular adaptations to flow. CFD simulations of the fetal heart, imaged by an echocardiogram, reveal complex flow patterns and the presence of flow vortex rings in both the left and right ventricles. These flow vortex rings generate significant WSS on the endocardium, potentially playing an important role in cardiac efficiency [13]. Indeed, CFD allows for the quantification of WSS, which is otherwise extremely difficult using only flow data measured in vivo.

Congenital coronary artery anomalies

Coronary artery anomalies (CAAs) accounts for 0.64% to 5.60% of patients undergoing coronary angiography [14], [15]. The pathophysiology and clinical history of the majority of CAAs have been fully clarified in the past 30 years. Myocardial bridges and anomalous origin from the opposite sinus (ACAOS) constitute the most clinically investigated pathologies among the wide spectrum of coronary artery anomalies, as they have been associated with myocardial infarction and sudden cardiac death [16].

Myocardial bridges (MB) were assessed by Javadzadegan et al. [17] using CFD by dividing patient-specific myocardial bridge models (n=10) by length. A direct relationship between myocardial bridge length and hemodynamic perturbations emerged in this study. Specifically, long myocardial bridge length seemed to be associated with lower WSS and higher residence time in the segment proximal to the bridge and a higher WSS and shorter residence time within the bridge, as compared to short length. More recently, Sharzehee M et al. [18] demonstrated that increasing the MB length (by 140%) only had a significant impact on the pressure drop in a severe MB (39% increase during exercise). However, increasing the stenosis length dramatically increased the pressure drop in both moderate and severe stenoses at all flow rates (31% and 93% increase during exercise, respectively). Both CFD and experimental results confirmed that the MB had a higher maximum and a lower mean pressure drop when compared to the stenosis, regardless of MB/stenosis severity.

The description of ACAOS is currently based on the terminology introduced by Angelini et al. [19], including an L or R prefix to indicate the (Right or Left) coronary artery involved and a suffix to indicate the proximal course: intramural (IM), pre-pulmonic (PP), subpulmonic (SP), retro-aortic (RA), retrocardiac (RC) and wrapped around the apex (WA). Rigatelli et al. computationally investigated the pathophysiology of Left ACAOS with and without an IM course [20]. After reviewing both the angiographic and computed tomography findings of 13 athletes, CFD models were created to simulate conditions reflecting extreme effort. In particular, vorticity magnitude, static pressure, and WSS were analyzed in models of L-ACAOS with no IM course and L-ACAOS-IM at rest and during exercise. The mean vorticity magnitude and WSS significantly increased from rest to exercise in both models in all the major coronary arteries. The mean static pressure (1.118e+004 vs 1.164e+004 Pa, $p < 0.001$), as well as the mean vorticity magnitude and mean WSS (7012.78

1/s vs 9019.56 1/s, $p < 0.001$, Δ=2006.78 1/s and 3.02 Pa vs 2.11 Pa, $p < 0.001$, Δ=0.91 Pa), significantly increased with exercise in the L-ACAOS-IM model. This net increment was transmitted to the entire left coronary system in the L-ACAOS-IM model but not in the L-ACAOS model with no IM. More recently, we analyzed the pathophysiology of L- and R- ACAOS with the IM course in relation to the eventual stenting of the IM course [21]. We theorized that the phasic squeezing phenomena inside IM could be produced by a combined mechanism of compression and twisting, which causes a net pressure drop leading to myocardial ischemia. This hypothesis seems to be confirmed in part by the study by Razavi et al. [22], which showed that different flow patterns exist natively between right and left anomalous coronary arteries. Unroofing may normalize time-averaged WSS, but with some differences related to the AO.

Interatrial shunts

Interatrial shunts include patent foramen ovale (PFO), secundum atrial septal defect (secundum ASD), sinus venosus ASD, and ostium primum ASD [23]. There are very few studies applying CFD to interatrial shunts. Our group investigated the pathophysiology of right-to-left shunting in patients with PFO with CFD [24]. In this study, we reconstructed the connection between the right and left atria using MRI data from a pool of patients with mild or permanent right-to-left shunting. In the CFD simulations, higher vorticity was observed in the case of permanent R-L shunt involving the wall of the left atrium (LA), especially at the left atrial appendage (LAA, Figure 2). On the contrary, when the severity of the shunt decreases, the vorticity in the same area is resultantly lower. Moreover, a marked gradient in total pressure (defined as the sum of static and dynamic pressures, measured in pascal (Pa)) was found across the PFO. A higher vorticity magnitude was observed in the permanent shunt both in the LA (117.32 vs. 110.25, p=0.001) and at the LAA (33.29 vs. 21.25, p=0.001) when compared to the trivial shunt.

Bicuspid aortic valve

Bicuspid aortic valve (BAV), usually associated with both valve dysfunction and aortic pathologies such as aortic dilatation and dissection, represents the most common CHD [25]. The abnormal arrangement of the aortic valve leaflets in BAV generates an abnormal flow pattern in the ascending aorta, depending on the type of leaflet fusion [26], [27]. Emendi et al. [28] demonstrated that fluid-structure interaction derived from MRI predicted the direction and magnitude of the flow jet impinging onto the aortic wall, as well as the location and extension of secondary flows and vortices developing at systole.

Rigatelli et al. suggested that such abnormal flow patterns, as evaluated by CFD, may be worsened by a concomitant coronary artery disease of proximal major coronary arteries, such as the left main stem, due to aberrant distribution of aortic WSS [29]. Some authors comparing the blood flow in BAV to that in normal (non-dilated) aortas with tricuspid
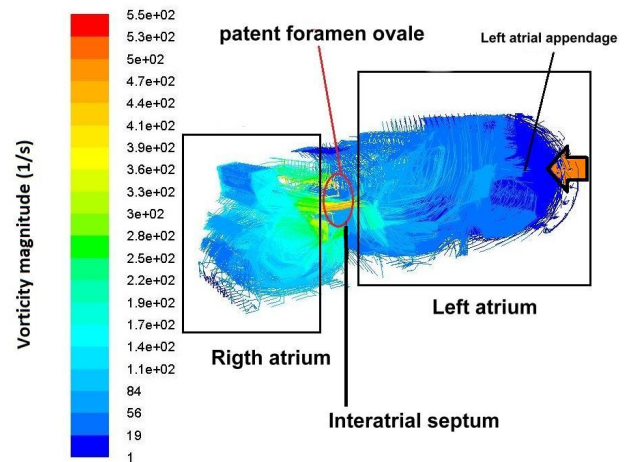

FIGURE 2. Computational fluid dynamic investigation of a patient with a high-grade Right-to-Left shunt (permanent shunt without Valsalva) through a patent foramen ovale, demonstrating a region of stagnant flow (blue) usually not present in patients with no shunt or mild shunt. Modified from Rigatelli G et al. [24]

aortic valves showed an altered WSS distribution in all different BAV fusion types [30], [31]. Both 4D-flow cardiovascular MRI and CFD analyses showed abnormal WSS distribution in patients with BAV even before aortic dilation occurred, suggesting that abnormal WSS could precede anatomical remodeling of the aorta. Thus, the monitoring of both WSS and aortic diameters has the potential to allow early identification of young, asymptomatic patients at risk for progression of aortopathy [32], guiding surgeons to reinforce the aortic sites at increased risk [26].

Coarctation of the aorta

Coarctation of the aorta (CoA) is a narrowing of the upper descending thoracic aorta, generally distal to the origin of the left subclavian artery and near the insertion of the ligamentum arteriosum. CoA accounts for approximately 5%–8% of all CHDs [33]. The available diagnostic imaging tools provide dimensions, velocities, and pressure gradients but cannot characterize aortic blood flow and its effects on the aortic wall. CFD, coupled with cardiac MRI, can offer a more comprehensive evaluation of the transaortic gradient, which is frequently uncorrected in sedated patients. Additionally, it may allow for the evaluation of blood flow patterns inside the aorta, as well as the potential effects of stenting or surgical repair [34].CFD has been used for surgical planning in clinical settings to aid surgeons and physicians in decision-making [35]-[37]. Models of each patient's anatomy after various types of surgery or stenting procedures can be generated, and CFD analyses based on patient-specific boundary conditions can assess the expected hemodynamics after intervention (Figure 4). Capelli et al. [38] used CFD to identify the maximum expansion diameter that would allow for effectively covered stent placement at the level of the narrowing while avoiding obstruction of the aberrant right subclavian artery and bronchial compression of the. The CFD
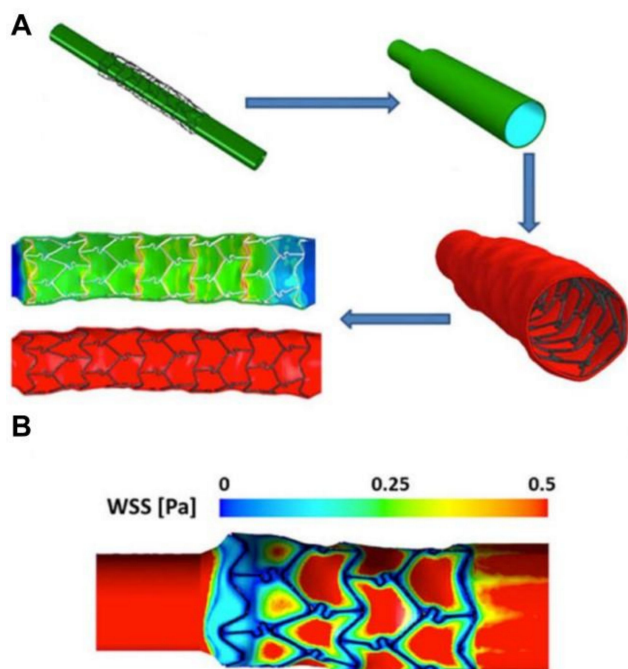
FIGURE 3. A computational fluid dynamics (CFD) model demonstrating the correlation between wall shear stress (WSS) and restenosis in coronary artery disease. (A) Structural modeling of stent insertion in porcine coronary arteries reconstructed from micro-CT, and stent–artery coupling obtained after arterial recoil. (C) Results of the CFD simulations in terms of the spatial distribution of WSS magnitude over the arterial wall. Modified from Morris PD et al. [3].

analyses are able to quantify the decrease in the peak velocity and pressure gradient, which in all the virtually-treated CoA patients dropped from an average of 15.5 mmHg pre-implant to 1.9 mmHg after stenting, predicting the results observed in real patients in the cath lab.

Tetralogy of Fallot

Tetralogy of Fallot (ToF) is characterized by pulmonary stenosis, ventricular septal defect, over-riding aorta, and right ventricle (RV) hypertrophy; ToF results in cyanosis and accounts for 7%–10% of all CHDs [39]. The surgical widening of the right ventricular outflow tract usually produces a certain degree of pulmonary valve regurgitation (PR), which can result in RV volume and pressure overload over time. PR could also play a role in the formation of vortex flow in PAs, although the aetiology is still poorly understood. In general, flow vortices are associated with alterations in WSS and affect endothelial function [40]. CFD could potentially identify parameters suitable for the prediction of outcomes in patients with repaired ToF and can define the timing for pulmonary valve replacement. Moreover, the coupling of CFD with virtual procedure simulation may be used to tailor possible percutaneous pulmonary valve implantation according to each patient's anatomy and flow patterns, as already demonstrated by Capelli et al. [38].

Univentricular heart

Patients with only a single functional ventricle usually are submitted to different palliative surgeries, resulting in a three-stage procedure [41], [42]: a) Norwood procedure [Blalock–Taussig shunts, central shunts, right ventricle-to-pulmonary artery conduit, and the hybrid Norwood], (b) Glenn or hemi-Fontan procedures, and (c) complete Fontan procedure (or total cavopulmonary connection) in which the superior and inferior caval veins are connected to the PA.

1) Norwood circulation

Migliavacca et al. [43] utilized CFD to investigate the Norwood circulation, evaluating the shunt pressure drop–flow relationships, as well as varying shunt implantation angles, diameters, curvatures, and input pulsatility values, and found that shunt diameter was the main determinant of graft flow (as expected). They demonstrated that most pressure drops occurred near the proximal anastomosis, and curved grafts resulted in a lower pressure drop compared to straight grafts due to reduced flow-line skewness towards the lateral graft wall near the proximal anastomosis. Subsequently, the same research group compared variants of the Norwood reconstructive surgeries with post-operative catheterization and Doppler data by carrying out a multi-scale CFD analysis [44]. A variation of the Norwood operation that utilized a modified Blalock–Taussig shunt was compared with the right ventricle-to-pulmonary artery shunt modification. The model predicted that the right ventricle shunt would result in higher aortic diastolic pressure, decreased pulmonary arterial pressure, lower pulmonary to systemic flow, and higher coronary perfusion relative to the innominate artery-to-right pulmonary artery shunt.

2) Fontan circulation

Assessment of the hemodynamic processes in Fontan circulation is difficult due to the abnormal position and geometry of the systemic ventricle, the extent of the Fontan circuit, and the passive nature of flow to pulmonary circulation. Blood flow to pulmonary circulation in Fontan patients is subjected to the peripheral muscle pump, systemic venous pressure, the systolic and diastolic performance of the systemic ventricle, and intrathoracic pressure changes during respiration. Recent research suggested that energy loss within the TCPC is an important factor in Fontan hemodynamics and should be decreased as much as possible via changes in vessel size, anastomosis shape, total blood flow, and pulmonary/caval flow distribution [45]. Haggerty et al. [46] used CMR-based CFD to evaluate the hemodynamics in 100 Fontan patients, with a focus on power loss within the Fontan circuit and demonstrated that Fontan tunnel stenosis and undersized pulmonary arteries are associated with increased power loss having a clear negative effect on Fontan hemodynamics.

CFD has been used to aid surgeons and physicians in clinical decision-making [47], providing insight into the pre-operative blood flow. Models of each patient's anatomy after

several different types of surgery can be virtually created, and patient-specific boundary conditions can be used to assess the expected hemodynamics after surgery.

CORONARY ARTERY PHYSIOLOGY

Stent rheology

CFD is currently being utilized to understand the impact of stent structure on coronary blood flow parameters. Several recent studies have suggested that the local geometric environment created by a deployed stent may influence regional blood flow characteristics and alter distributions of wall shear stress (WSS) after implantation, thereby creating the conditions by which some specific areas of the vessel wall can be more susceptible to neointimal hyperplasia, and restenosis [48]. Stents are most frequently implanted in curved vessels such as the coronary arteries, but most computational studies examining blood flow patterns through stented vessels use linear, cylindrical geometric models (Figure 3). It is likely that restenosis after stent implantation in curved arteries also occurs as a consequence of changes in fluid dynamics that are created after stent implantation. Ladisa et al. [49] found that the time-averaged WSS in the proximal portion of the stent ranged from 8.91 to 11.7 dynes/cm^2 along the pericardial luminal surface and 4.26 to 4.88 dynes/cm^2 along the myocardial luminal surface of curved coronary arteries, compared to 8.31 dynes/cm^2 observed throughout the stented region of a straight vessel implanted with an equivalent stent. The same group hypothesized that channeling of adjacent blood layers would have a profound effect on wall shear stress due to stent geometry [50]. Stagnation zones are usually localized in the proximity of stent struts. Minimum WSS decreased by 77% in stented compared to unstented vessels. Regions of low WSS were extended at the stent outlet and localized to regions where adjacent axial strut spacing was minimized, and the circumferential distance between struts was huge. These preliminary results have been confirmed by different authors [51], [52], who also suggested that stents with a helical configuration generated an extra swirling component of the flow in a helical direction without significant changes to the distribution of WSS.

Coronary bifurcation

One of the most valuable applications of CFD in coronary artery research is in the study of coronary artery bifurcations, particularly that of the left main bifurcation. CFD was used to anticipate the results of complex bifurcation stenting and to understand how bifurcation rheology changes following stenting with various devices and techniques.

Chen et al. [48] showed that stenting of the main vessel increased the maximum CWS in the side branch (SB), resulting in a nearly two-fold increase in the stress ratio in the SB compared to the MB (5.1 × 105 vs. 9.2 × 105). The existence of plaque decreased WSS and increased CWS near the carina, increasing the stress ratio at the SB. The changes in the stress ratio were highly consistent with clinical data on bifurcation stenting. Similarly, other investigations
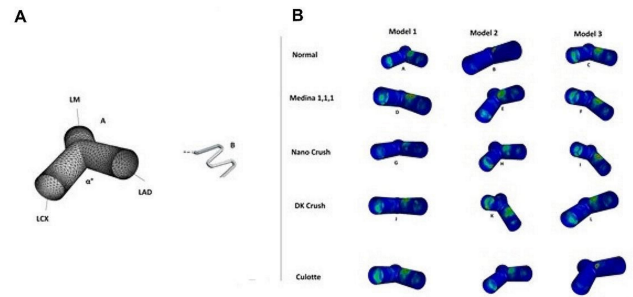

FIGURE 4. Panel A: Stented left main bifurcation: the model after a stenting procedure (a) using a third generation 80-micron drug-eluting stent (b). Panel B: Tridimensional evaluation of WSS in three angles configurations: model 1 (45°), model 2 (60°), and model 3 (80°) in the physiologic (normal) and pathologic (Medina 1,1,1) states and after simulating the three dual stenting techniques, Nano crush, DK crush, and Culotte. In Model 1, the Nano crush technique leads to a substantial improvement of the WSS on both the LAD and LCX walls. Conversely, a less physiological WSS reduction was obtained at the same artery sites using the DK and culotte techniques, respectively. In model 2, despite a good improvement of the WSS using the Nanocrush approach, an area of lower WSS was still present after the stenting in the inferior roof of the LCX, probably due to a non-optimal stent apposition at that angle. The same area of lower WSS was also present after the DK stenting, but this was located more centrally on the vessel wall. Conversely, the use of the Culotte stenting removed this area. In model 3, areas with intermediate values of WSS were still present in the LCX after the stenting with the Nano-crush and culotte techniques. However, the DK crush allows for the obtainment of more physiological values of WSS in the LAD wall. Similarly, the culotte stenting leads to an acceptable physiological WSS configuration in the bifurcation model. Modified from Rigatelli G et al. [53]

have suggested that angles of bifurcation [54] and stenting technique may differently impact stent rheology, potentially influencing the risk of restenosis and thrombosis based on the amount of metal struts placed into the carina [55], [56] (Figure 4). Another variable considered was the site for the proximal optimization technique, which has a major role in determining the surface of the area corresponding with lower WSS. CFD has also been used to determine the risk of occlusion in patients with subclinical disease of the Left main or other bifurcation sites, suggesting a correlation between WSS in pre-existing coronary disease and the risk of acute closure of the vessel [57].

ATHEROSCLEROSIS DISEASE PROGRESSION

CFD has been recently applied to the pathophysiology of atherosclerosis in order to understand the mechanisms underlying plaque progression and rupture. In particular, recent studies have focused on the mechanism referred to as "cavitation."

From a physical point of view, cavitation occurs when the pressure (P) in an area of flowing fluid decreases below that of the vapor pressure (Pv). More precisely, cavitation bubbles form immediately below the Pv level, reaching their highest velocity at the lowest pressure level (Pmin), which is also known as the vena contracta point. Subsequently, bubbles increase in size with increasing pressure, leading to bubble collapse above the Pv level. This phenomenon is the result of two separate processes, which represent the essential substrates of cavitation: the former is represented
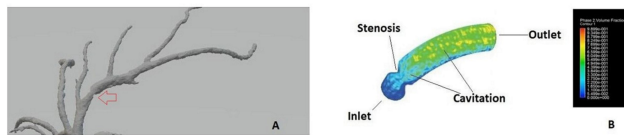
FIGURE 5. Three-Dimensional reconstruction model of a left coronary artery from a cardiac CT. (A)The stenosis is marked with a red arrow. (B) Demonstration of cavitation in concentric stenosis.
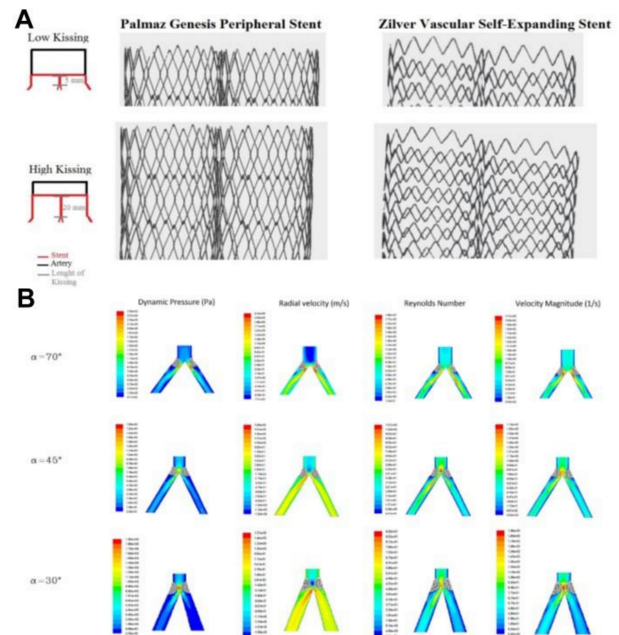

FIGURE 6. Aortoiliac virtual simulation of different kissing stent configurations. (A) Schematic representation of the height of kissing applied to the analysis. Arterial walls have been subtracted to better represent the stent interactions. (B) Profile of the stenosis on the iliac artery bifurcation model with respect to the different fluid parameters considered in the analysis. Modified from Rigatelli G et al. [63]

by a large pressure fluctuation (dp/dt), while the latter is due to turbulent flow.

CFD studies demonstrated that cavitation is generated by both concentric and eccentric coronary artery stenosis (75% for the former and 50% for the latter), which propagates downstream of the vessel, creating microbubbles that ruptured when the fluid pressure is lower than the vapor pressure at a local thermodynamic state [58](Figure 5). Biomechanically, cavitation might damage endothelial surfaces and promote thrombosis.

The cavitation phenomenon alone is not sufficient to explain the growth, structural changes, and biochemical modifications in coronary atherosclerotic plaques, but it may act as a concurrent, rather than causal, factor in the precipitation of atherosclerotic disease.

PERIPHERAL VASCULAR DISEASE

The peripheral vascular disease has begun to become a field of interest for CFD application. CFD has been applied to abdominal aortic aneurysms to predict aneurysm progression and risk of rupture, and it also has been used in the prediction of the putative therapeutic effects of endovascular repair [59], [60]. CFD has additionally been utilized to study aortic dissection, where computed pressure and flow conditions can be used to guide (semi-) invasive therapeutic procedure decisions. The physiological effects of therapies can thus be simulated, and anticipated [61], [62]. CFD has been recently adopted in peripheral artery disease, particularly in femoral and aortoiliac vascular districts, to anticipate the impact on WSS of different stent types and configurations [63] (Figure 6).

CONCLUSION

Further improvement in the quality of available virtual simulation software and its integration with existing diagnostic tools such as MRI, 3D, and 4D ultrasound, optical coherence tomography, intravascular ultrasound imaging, and angiography are likely to push CFD forward in clinical practice. As a result, the transition from offline assessment and planning to online evaluation and treatment will likely become much more effective.

FUNDING

DECLARATION OF INTEREST

The authors have no relevant affiliations or financial involvement with any organization or entity with a financial interest or financial conflict with the subject matter or materials discussed in the manuscript. This includes employment, consultancies, honoraria, stock ownership or options, expert testimony, grants or patents received or pending, or royalties.

REFERENCES

[1] Taylor CA, Figueroa CA "Patient-specific modeling of cardiovascular mechanics." Annual Review of Biomedical Engineering, Sep. 2009, 11:109–134, DOI: 10.1146/annurev.bioeng.10.061807.160521, PMID: 19400706.

[2] Morris PD, Ryan D, Morton AC et al. "Virtual fractional flow reserve from coronary angiography: modeling the significance of coronary lesions: results from the VIRTU-1 (VIRTUal Fractional Flow Reserve From Coronary Angiography) study." JACC. Cardiovascular Interventions, Feb. 2013, 6:149–157, DOI: 10.1016/j.jcin.2012.08.024, PMID: 23428006.

[3] Morris PD, Narracott A, von Tengg-Kobligk H et al. "Computational fluid dynamics modelling in cardiovascular medicine." Heart (British Cardiac Society), Jan. 2016, 102:18–28, DOI: 10.1136/heartjnl-2015-308044, PMID: 26512019.

[4] Theodorakakos A, Gavaises M, Andriotis A et al. "Simulation of cardiac motion on non-Newtonian, pulsating flow development in the human left anterior descending coronary artery." Physics in Medicine and Biology, Sep. 2008, 53:4875–4892, DOI: 10.1088/0031-9155/53/18/002, PMID: 18711245.

[5] Cho YI, Kensey KR "Effects of the non-Newtonian viscosity of blood on flows in a diseased arterial vessel. Part 1: Steady flows." Biorheology, 1991, 28:241–262, DOI: 10.3233/bir-1991-283-415, PMID: 1932716.

[6] Pennati G, Corsini C, Hsia TY et al. "Computational fluid dynamics models and congenital heart diseases." Frontiers in Pediatrics, Feb. 2013, 1:4, DOI: 10.3389/fped.2013.00004, PMID: 24432298.

[7] Arbia G, Corsini C, Esmaily Moghadam M et al. "Numerical blood flow simulation in surgical corrections: what do we need for an accurate analysis?" The Journal of Surgical Research, Jan. 2014, 186:44–55, DOI: 10.1016/j.jss.2013.07.037, PMID: 23993199.

[8] Jamalidinan F, Hassanabad AF, François CJ et al. "Four-dimensional-flow Magnetic Resonance Imaging of the Aortic Valve and Thoracic Aorta." Radiologic Clinics of North America, Jul. 2020, 58:753–763, DOI: 10.1016/j.rcl.2020.02.008, PMID: 32471542.

[9] Morbiducci U, Kok AM, Kwak BR et al. "Atherosclerosis at arterial bifurcations: evidence for the role of haemodynamics and geometry." Thrombosis and Haemostasis, Mar. 2016, 115:484–492, DOI: 10.1160/TH15-07-0597, PMID: 26740210.

[10] Lindsey SE, Butcher JT, Yalcin HC "Mechanical regulation of cardiac development." Frontiers in Physiology, 2014, 5:318, DOI: 10.3389/fphys.2014.00318, PMID: 25191277.

[11] Sato Y, Poynter G, Huss D et al. "Dynamic analysis of vascular morphogenesis using transgenic quail embryos." PloS One, Sep. 2010, 5:e12674, DOI: 10.1371/journal.pone.0012674, PMID: 20856866.

[12] Hierck BP, Van der Heiden K, Poelma C et al. "Fluid Shear Stress and Inner Curvature Remodeling of the Embryonic Heart. Choosing the Right Lane!" The Scientific World JOURNAL, 2008, 8:939501, DOI: 10.1100/tsw.2008.42. [Online]. Available: https://doi.org/10.1100/tsw.2008.42

[13] Courchaine K, Rugonyi S "Quantifying blood flow dynamics during cardiac development: demystifying computational methods." Philosophical Transactions of the Royal Society of London. Series B, Biological sciences, Sep. 2018, 373, DOI: 10.1098/rstb.2017.0330, PMID: 30249779.

[14] Kardos A, Babai L, Rudas L et al. "Epidemiology of congenital coronary artery anomalies: a coronary arteriography study on a central European population." Catheterization and Cardiovascular Diagnosis, Nov. 1997, 42:270–275, DOI: 10.1002/(sici)1097-0304(199711)42:3<270::aid-ccd8>3.0.co;2-9, PMID: 9367100.

[15] Yamanaka O, Hobbs RE "Coronary artery anomalies in 126,595 patients undergoing coronary arteriography." Catheterization and Cardiovascular Diagnosis, Sep. 1990, 21:28–40, DOI: 10.1002/ccd.1810210110, PMID: 2208265.

[16] Rigatelli G, Rigatelli A, Cominato S et al. "A clinical-angiographic risk scoring system for coronary artery anomalies." Asian Cardiovascular Thoracic Annals, Jun. 2012, 20:299–303, DOI: 10.1177/0218492312437880, PMID: 22718718.

[17] Javadzadegan A, Moshfegh A, Fulker D et al. "Development of a Computational Fluid Dynamics Model for Myocardial Bridging." Journal of Biomechanical Engineering, Sep. 2018, 140, DOI: 10.1115/1.4040127, PMID: 29801175.

[18] Sharzehee M, Seddighi Y, Sprague EA et al. "A Hemodynamic Comparison of Myocardial Bridging and Coronary Atherosclerotic Stenosis: A Computational Model With Experimental Evaluation." Journal of Biomechanical Engineering, Mar. 2021, 143, DOI: 10.1115/1.4049221, PMID: 33269788.

[19] Angelini P, Uribe C "Anatomic spectrum of left coronary artery anomalies and associated mechanisms of coronary insufficiency." Catheterization and Cardiovascular Interventions : Official Journal of The Society for Cardiac Angiography Interventions, Aug. 2018, 92:313–321, DOI: 10.1002/ccd.27656, PMID: 30051621.

[20] Rigatelli G, Zuin M, Galasso P et al. "Mechanisms of Myocardial Ischemia Inducing Sudden Cardiac Death in Athletes with Anomalous Coronary Origin from the Opposite Sinus: Insights from a computational fluid dynamic study." Cardiovascular Revascularization Medicine : Including Molecular Interventions, Dec. 2019, 20:1112–1116, DOI: 10.1016/j.carrev.2019.01.031, PMID: 30808598.

[21] Rigatelli G, Zuin M "Computed Tomography-based Patient-specific Biomechanical and Fluid Dynamic Study of Anomalous Coronary Arteries with Origin from the Opposite Sinus and Intramural Course," Heart International, 2020.

[22] Razavi A, Sachdeva S, Frommelt PC et al. "Patient-Specific Numerical Analysis of Coronary Flow in Children With Intramural Anomalous Aortic Origin of Coronary Arteries." Seminars in Thoracic and Cardiovascular Surgery, 2021, 33:155–167, DOI: 10.1053/j.semtcvs.2020.08.016, PMID: 32858220.

[23] Rigatelli G, Zuin M, Nghia NT "Interatrial shunts: technical approaches to percutaneous closure." Expert Review of Medical Devices, Oct. 2018, 15:707–716, DOI: 10.1080/17434440.2018.1526674, PMID: 30246569.

[24] Rigatelli G, Zuin M, Fong A "Computational Flow Dynamic Analysis of Right and Left Atria in Patent Foramen Ovale: Potential Links with Atrial Fibrillation." Journal of Atrial Fibrillation, Feb. 2018, 10:1852, DOI: 10.4022/jafib.1852, PMID: 29988264.

[25] Yener N, Oktar GL, Erer D et al. "Bicuspid aortic valve." Annals of Thoracic and Cardiovascular Surgery : Official journal of the Association of Thoracic and Cardiovascular Surgeons of Asia, Oct. 2002, 8:264–267, PMID: 12472407.

[26] Piatti F, Sturla F, Bissell MM et al. "4D Flow Analysis of BAV-Related Fluid-Dynamic Alterations: Evidences of Wall Shear Stress Alterations in Absence of Clinically-Relevant Aortic Anatomical Remodeling." Frontiers in Physiology, 2017, 8:441, DOI: 10.3389/fphys.2017.00441, PMID: 28694784.

[27] Meierhofer C, Schneider EP, Lyko C et al. "Wall shear stress and flow patterns in the ascending aorta in patients with bicuspid aortic valves differ significantly from tricuspid aortic valves: a prospective study." European Heart Journal. Cardiovascular Imaging, Aug. 2013, 14:797–804, DOI: 10.1093/ehjci/jes273, PMID: 23230276.

[28] Emendi M, Sturla F, Ghosh RP et al. "Patient-Specific Bicuspid Aortic Valve Biomechanics: A Magnetic Resonance Imaging Integrated Fluid-Structure Interaction Approach." Annals of Biomedical Engineering, Feb. 2021, 49:627–641, DOI: 10.1007/s10439-020-02571-4, PMID: 32804291.

[29] Rigatelli G, Zuin M, Fong A et al. "Left Main Stenting Induced Flow Disturbances on Ascending Aorta and Aortic Arch." Journal of Translational Internal Medicine, Mar. 2019, 7:22–28, DOI: 10.2478/jtim-2019-0005, PMID: 30997353.

[30] Cao K, Atkins SK, McNally A et al. "Simulations of morphotype-dependent hemodynamics in non-dilated bicuspid aortic valve aortas." Journal of Biomechanics, Jan. 2017, 50:63–70, DOI: 10.1016/j.jbiomech.2016.11.024, PMID: 27855987.

[31] McNally A, Madan A, Sucosky P "Morphotype-Dependent Flow Characteristics in Bicuspid Aortic Valve Ascending Aortas: A Benchtop Particle Image Velocimetry Study." Frontiers in Physiology, 2017, 8:44, DOI: 10.3389/fphys.2017.00044, PMID: 28203207.

[32] Ando M, Okita Y, Morota T et al. "Thoracic aortic aneurysm associated with congenital bicuspid aortic valve." Cardiovascular Surgery (London, England), Dec. 1998, 6:629–634, DOI: 10.1016/s0967-2109(98)00094-5, PMID: 10395268.

[33] Michelena HI, Prakash SK, Della Corte A et al. "Bicuspid aortic valve: identifying knowledge gaps and rising to the challenge from the International Bicuspid Aortic Valve Consortium (BAVCon)." Circulation, Jun. 2014, 129:2691–2704, DOI: 10.1161/CIRCULATIONAHA.113.007851, PMID: 24958752.

[34] Riesenkampff E, Fernandes JF, Meier S et al. "Pressure fields by flow-sensitive, 4D, velocity-encoded CMR in patients with aortic coarctation." JACC. Cardiovascular Imaging, Sep. 2014, 7:920–926, DOI: 10.1016/j.jcmg.2014.03.017, PMID: 25212797.

[35] Arzani A, Dyverfeldt P, Ebbers T et al. "In vivo validation of numerical prediction for turbulence intensity in an aortic coarctation." Annals of Biomedical Engineering, Apr. 2012, 40:860–870, DOI: 10.1007/s10439-011-0447-6, PMID: 22016327.

[36] LaDisa JFJ, Alberto Figueroa C, Vignon-Clementel IE et al. "Computational simulations for aortic coarctation: representative results from a sampling of patients." Journal of Biomechanical Engineering, Sep. 2011, 133:91008, DOI: 10.1115/1.4004996, PMID: 22010743.

[37] LaDisa JFJ, Dholakia RJ, Figueroa CA et al. "Computational simulations demonstrate altered wall shear stress in aortic coarctation patients treated by resection with end-to-end anastomosis," Congenital Heart Disease, 2011, 6:432–443, DOI: https://doi.org/10.1111/j.1747-0803.2011.00553.x. [Online]. Available: https://onlinelibrary.wiley.com/doi/abs/10.1111/j.1747-0803.2011.00553.x

[38] Capelli C, Sauvage E, Giusti G et al. "Patient-specific simulations for planning treatment in congenital heart disease." Interface Focus, Feb. 2018, 8:20170021, DOI: 10.1098/rsfs.2017.0021, PMID: 29285347.

[39] Villafañe J, Feinstein JA, Jenkins KJ et al. "Hot topics in tetralogy of Fallot." Journal of the American College of Cardiology, Dec. 2013, 62:2155–2166, DOI: 10.1016/j.jacc.2013.07.100, PMID: 24076489.

[40] Paszkowiak JJ, Dardik A "Arterial wall shear stress: observations from the bench to the bedside." Vascular and Endovascular Surgery, 2003, 37:47–57, DOI: 10.1177/153857440303700107, PMID: 12577139.

[41] Fontan F, Baudet E "Surgical repair of tricuspid atresia." Thorax, May. 1971, 26:240–248, DOI: 10.1136/thx.26.3.240, PMID: 5089489.

[42] Galantowicz M, Cheatham JP, Phillips A et al. "Hybrid approach for hypoplastic left heart syndrome: intermediate results after the learning curve." The Annals of Thoracic Surgery, Jun. 2008, 85:2061–2063, DOI: 10.1016/j.athoracsur.2008.02.009, PMID: 18498821.

[43] Migliavacca F, Pennati G, Dubini G et al. "Modeling of the Norwood circulation: effects of shunt size, vascular resistances, and heart rate." American Journal of Physiology. Heart and Circulatory Physiology, May.

2001, 280:H2076–86, DOI: 10.1152/ajpheart.2001.280.5.H2076, PMID: 11299209.

[44] Migliavacca F, Balossino R, Pennati G et al."Multiscale modelling in biofluidynamics: application to reconstructive paediatric cardiac surgery." Journal of Biomechanics, 2006, 39:1010–1020, DOI: 10.1016/j.jbiomech.2005.02.021, PMID: 16549092.

[45] Rijnberg FM, Hazekamp MG, Wentzel JJ et al."Energetics of Blood Flow in Cardiovascular Disease: Concept and Clinical Implications of Adverse Energetics in Patients With a Fontan Circulation." Circulation, May. 2018, 137:2393–2407, DOI: 10.1161/CIRCULATIONAHA.117.033359, PMID: 29844073.

[46] Haggerty CM, Restrepo M, Tang E et al."Fontan hemodynamics from 100 patient-specific cardiac magnetic resonance studies: a computational fluid dynamics analysis." The Journal of Thoracic and Cardiovascular Surgery, Oct. 2014, 148:1481–1489, DOI: 10.1016/j.jtcvs.2013.11.060, PMID: 24507891.

[47] Trusty PM, Restrepo M, Kanter KR et al."A pulsatile hemodynamic evaluation of the commercially available bifurcated Y-graft Fontan modification and comparison with the lateral tunnel and extracardiac conduits." The Journal of Thoracic and Cardiovascular Surgery, Jun. 2016, 151:1529–1536, DOI: 10.1016/j.jtcvs.2016.03.019, PMID: 27056758.

[48] Chen HY, Chatzizisis YS, Louvard Y et al."Computational Simulations of Provisional Stenting of a Diseased Coronary Artery Bifurcation Model." Scientific Reports, Jun. 2020, 10:9667, DOI: 10.1038/s41598-020-66777-1, PMID: 32541660.

[49] LaDisa JF, Olson LE, Douglas HA et al."Alterations in regional vascular geometry produced by theoretical stent implantation influence distributions of wall shear stress: analysis of a curved coronary artery using 3D computational fluid dynamics modeling," BioMedical Engineering OnLine, 2006, 5:40, DOI: 10.1186/1475-925X-5-40. [Online]. Available: https://doi.org/10.1186/1475-925X-5-40

[50] LaDisa JFJ, Guler I, Olson LE et al."Three-dimensional computational fluid dynamics modeling of alterations in coronary wall shear stress produced by stent implantation." Annals of Biomedical Engineering, Sep. 2003, 31:972–980, DOI: 10.1114/1.1588654, PMID: 12918912.

[51] Martin DM, Murphy EA, Boyle FJ"Computational fluid dynamics analysis of balloon-expandable coronary stents: influence of stent and vessel deformation." Medical Engineering Physics, Aug. 2014, 36:1047–1056, DOI: 10.1016/j.medengphy.2014.05.011, PMID: 24953569.

[52] Chen WX, Poon EKW, Hutchins N et al."Computational fluid dynamics study of common stent models inside idealised curved coronary arteries." Computer Methods in Biomechanics and Biomedical Engineering, May. 2017, 20:671–681, DOI: 10.1080/10255842.2017.1289374, PMID: 28349764.

[53] Rigatelli G, Zuin M NT"Left main bifurcation stenting assessed by computational fluid dynamic: The impact on wall shear stress forces depends on both specific techniques and bifurcation angles." Journal of Integrative Cardiology, 2018, 4:1–7, DOI: https://doi.org/10.15761/jic.1000259.

[54] Sun Z, Chaichana T"An investigation of correlation between left coronary bifurcation angle and hemodynamic changes in coronary stenosis by coronary computed tomography angiography-derived computational fluid dynamics." Quantitative Imaging in Medicine and Surgery, Oct. 2017, 7:537–548, DOI: 10.21037/qims.2017.10.03, PMID: 29184766.

[55] Zuin M, Rigatelli G, Chiastra C"Optimal Site for Proximal Optimization Technique in Complex Coronary Bifurcation Stenting: A Computational Fluid Dynamics Study." Cardiovascular Revascularization Medicine : Including Molecular Interventions, Jul. 2020, 21:826–832, DOI: 10.1016/j.carrev.2019.12.015, PMID: 31866275.

[56] Rigatelli G, Zuin M, Dell'Avvocata F et al."Evaluation of coronary flow conditions in complex coronary artery bifurcations stenting using computational fluid dynamics: Impact of final proximal optimization technique on different double-stent techniques." Cardiovascular Revascularization Medicine : Including Molecular Interventions, Jun. 2017, 18:233–240, DOI: 10.1016/j.carrev.2017.01.002, PMID: 28108202.

[57] Zuin M, Rigatelli G, Vassilev D et al."Computational fluid dynamic-derived wall shear stress of non-significant left main bifurcation disease may predict acute vessel thrombosis at 3-year follow-up." Heart and Vessels, Mar. 2020, 35:297–306, DOI: 10.1007/s00380-019-01494-y, PMID: 31482218.

[58] Rigatelli G, Zuin M, Ngo TT et al."Intracoronary Cavitation as a Cause of Plaque Rupture and Thrombosis Propagation in Patients with Acute Myocardial Infarction: A Computational Study." Journal of Translational Internal Medicine, Jun. 2019, 7:69–75, DOI: 10.2478/jtim-2019-0014, PMID: 31380239.

[59] Georgakarakos E, Ioannou CV, Papaharilaou Y et al."Computational evaluation of aortic aneurysm rupture risk: what have we learned so far?" Journal of Endovascular Therapy : An Official Journal of the International Society of Endovascular Specialists, Apr. 2011, 18:214–225, DOI: 10.1583/10-3244.1, PMID: 21521062.

[60] Molony DS, Kavanagh EG, Madhavan P et al."A computational study of the magnitude and direction of migration forces in patient-specific abdominal aortic aneurysm stent-grafts." European Journal of Vascular and Endovascular surgery : the official journal of the European Society for Vascular Surgery, Sep. 2010, 40:332–339, DOI: 10.1016/j.ejvs.2010.06.001, PMID: 20573524.

[61] Karmonik C, Müller-Eschner M, Partovi S et al."Computational fluid dynamics investigation of chronic aortic dissection hemodynamics versus normal aorta." Vascular and Endovascular Surgery, Nov. 2013, 47:625–631, DOI: 10.1177/1538574413503561, PMID: 24048257.

[62] Chen D, Müller-Eschner M, von Tengg-Kobligk H et al."A patient-specific study of type-B aortic dissection: evaluation of true-false lumen blood exchange." Biomedical Engineering Online, Jul. 2013, 12:65, DOI: 10.1186/1475-925X-12-65, PMID: 23829346.

[63] Rigatelli G, Zuin M, Dell'Avvocata F et al."Non-invasive Evaluation of Fluid Dynamic of Aortoiliac Atherosclerotic Disease: Impact of Bifurcation Angle and Different Stent Configurations." Journal of Translational Internal Medicine, Sep. 2018, 6:138–145, DOI: 10.2478/jtim-2018-0020, PMID: 30425950.